
Article:
Bovill, E., Scarratt, N., Griffin, J. et al. (5 more authors) (2015) The role of the hole-extraction layer in determining the operational stability of a polycarbazole: fullerene bulk-heterojunction photovoltaic device. Applied Physics Letters, 106 (7). ISSN 0003-6951

https://doi.org/10.1063/1.4909530

The role of the hole-extraction layer in determining the operational stability of a polycarbazole:fullerene bulk-heterojunction photovoltaic device

E. Bovill[1], N. Scarratt[1], J. Griffin[1], H. Yi[2], A. Iraqi[2], A.R. Buckley[1], J.W. Kingsley[3], D.G. Lidzey[1]*

[1] Department of Physics and Astronomy, University of Sheffield, Sheffield, S3 7RH, UK

[2] Department of Chemistry, University of Sheffield, Sheffield, S3 7HF, UK

[3] Ossila Ltd., Kroto Innovation Centre, Broad Lane, Sheffield, S3 7HQ, UK

* Corresponding author: d.g.lidzey@sheffield.ac.uk

Abstract

We have made a comparative study of the relative operational stability of bulk-heterojunction organic photovoltaic (OPV) devices utilising different hole transport layers (HTLs). OPV devices were fabricated based on a blend of the polymer PCDTBT with the fullerene $PC_{70}BM$, and incorporated the different HTL materials PEDOT:PSS, MoO_x and V_2O_5. Following 620 hours of irradiation by light from a solar simulator, we find that devices using the PEDOT:PSS HTL retained the highest efficiency, having a projected T_{80} lifetime of 14,500 hours.

The commercialisation of polymer:fullerene bulk-heterojunction photovoltaics will require the demonstration of high device efficiency together with extended device lifetime. Indeed, it has been estimated [1], that it will be necessary for organic photovoltaic devices (OPVs) to demonstrate power conversion efficiencies (PCE) and operational lifetimes of 10% and 10 years respectively before commercialisation is possible. Following recent advances in device efficiency, attention has increasingly focused on OPV lifetime and the mechanisms that underpin device degradation [2]. Much work on degradation processes have studied OPV devices based on the material poly(3-hexylthiophene) (P3HT) [3–6], with lifetimes of up to 3 years reported [6]. More recently, outdoor inter-laboratory studies on P3HT based devices reveal extrapolated lifetimes in excess of 5 years [7], with other laboratory studies on poly[9-(heptadecan-9-yl)-9H-carbazole-2,7-diyl-alt-(4′,7′-di-2-thienyl-2′,1′,3′-benzothiadiazole)-5,5-diyl] [PCDTBT] based OPVs demonstrating extrapolated device lifetimes of up to 10 years [6,8].

To improve OPV stability and lifetime, several studies now report the effect of changing other interlayers within P3HT based devices [9–12]. Notably, PCDTBT [6,11,12,18] and other polycarbazole polymers can be used to create devices having extended operational lifetimes [6], with the comparative stability afforded by PCDTBT presenting an opportunity to determine the relative role of the hole transport layer (HTL) in contributing to device stability. We have therefore fabricated PCDTBT:$PC_{70}BM$ OPV devices that utilise a range of HTLs including poly(3,4-ethylenedioxythiophene):poly(styrene sulfonic acid) (PEDOT:PSS), molybdenum oxide (MoO_x) and vanadium oxide (V_2O_5) and have measured device PCE under simulated solar radiation over a period of 620 hours. We find that in contrast to previous work [9,10,12], devices utilising a PEDOT:PSS HTL have higher stability that those incorporating MoO_x or V_2O_5 HTLs, having an extrapolated T_{80} lifetime of 14,500 hours.

The devices explored are based on the structure ITO/HTL/PCDTBT:$PC_{70}BM$/Ca/Al in which the hole transport layer was composed of MoO_x, PEDOT:PSS or V_2O_5. PEDOT:PSS is a material that has been widely explored as a hole-transporting layer due to its large work-function, high conductivity and good film transparency [19]. Thin films of PEDOT:PSS are however extremely hygroscopic [20], and post deposition thermal treatments are needed to remove water remaining in the films.

MoO_x, along with other transition metals, has been used extensively with polymers having low lying HOMO levels to improve charge extraction due to its large work function (in the region of 5.5 eV [21]). MoO_x can be deposited by a variety of processes, including evaporation [22], sputtering [23] and solution-based deposition [24–26]. When combined with polymers having a deep HOMO level,

such as PCDTBT (-5.5eV [27]), device efficiencies of over 7% have been achieved [12]. In this study we have used thermally-evaporated MoO_x; a form of this metal oxide most often utilised in OPVs.

V_2O_5 is a transition metal oxide that has been extensively used as a HTL in OPVs. It can be deposited by a variety of processes and has a work function of 5.6 eV [28] making it well matched for hole extraction from PCDTBT. To deposit V_2O_5, we have used a facile synthetic process in air to form uniform thin layers of V_2O_5 from an oxytriisopropoxide precursor solution [29–31], forming an amorphous, smooth V_2O_5 layer.

OPV devices were fabricated on ITO substrates provided by Ossila Ltd. Devices utilising a PEDOT:PSS HTL (Heraeus Clevios™ P VP AI 4083) layer were spin-cast at to form a ~ 30 nm thick film which were annealed for 10 minutes at 150°C, following which they were transferred to a nitrogen filled glovebox. The MoO_x HTLs were deposited by thermal evaporation, using molybdenum (VI) oxide pellets placed in an aluminium oxide crucible. Vanadium oxytriisopropoxide was dissolved in 2-propanol at a concentration of 5 µL/mL and spin cast in air to form a ~ 5 nm thick thin film. The film was left in air for 45 minutes to fully hydrolyse, after which it was transferred to a glovebox for further processing.

The active layer of all devices was deposited from a solution of PCDTBT (synthesised using previously described techniques [32]) blended with $PC_{70}BM$ at a total concentration of 25 mg mL^{-1} at 1:4 blend ratio in chlorobenzene. This active layer solution was spin-cast onto each HTL layer in the glovebox to form a 70 nm thick film. A cathode consisting of a calcium / aluminium film (5 / 100 nm) was then thermally evaporated onto the active layer creating 6 pixels on each substrate, each having an active area of 0.04 cm^2. Finally, the devices were encapsulated using a glass cover slip and a UV-curable epoxy in the glovebox.

The completed devices were measured using a Newport 92251A-1000 AM 1.5 solar simulator calibrated against an NREL certified silicon reference cell. An aperture mask having an area of 0.0261 cm^2 was used to define the area irradiated on each pixel. The values of PCE, J_{sc}, FF and V_{oc} we quote represent an average of parameters recorded from 12 pixels defined on two separate substrates in which the worst 25% of pixels have been omitted. The errors quoted are defined by the standard deviation about the mean. External quantum efficiency (EQE) measurements were made using a halogen lamp as a light source in conjunction with a monochromator. A Newport 818-UV calibrated silicon photodiode was used to measure a reference spectrum of the light source.

Lifetime testing was carried out in an ATLAS Suntest CPS+ solar simulator with a 1500 W xenon lamp in which a quartz filter was used to reduce the IR portion of the emitted light and more closely replicate the solar spectrum. Note that devices placed in the ATLAS solar simulator were

not covered by an aperture mask during irradiation or during JV testing. Internal reflectors in the ATLAS test chamber were used to produce a uniform light irradiation of 1000 Wm^{-2} over all the devices, with differences in the light flux impinging on the different OPV devices being less than 3%. The temperature inside the ATLAS testing chamber was held at (40 ± 2)°C. A series of temperature sensors placed over the device test area indicated that variations in the temperature between different devices was < 1°C. The typical humidity in the lifetime testing system was (25 ± 5)%. A photograph of the OPV test-board, temperature sensors and reference photodiodes is shown in **Figure 1 (a)**.

We have characterised the spectral distribution of the radiation inside the ATLAS solar simulator as shown in **Figure 1 (b)**, and find a reasonably close correspondence between the ATLAS and the AM1.5 solar spectrum over the wavelength range 350 - 600 nm, corresponding to the absorption maxima of the polymer:fullerene active layer. However, small differences in the spectra resulted in a difference in OPV J_{sc} measured using the different systems of ≤ 10%. To eliminate errors resulting from the spectral mismatch, all tabulated device metrics quoted (PCE, FF, V_{oc}, J_{sc} and T_{80}) were determined from separate JV scans measured using an aperture mask and the calibrated Newport solar simulator.

In our measurements, we made a side-by-side comparison between six devices based on PEDOT:PSS, MoO_x and V_2O_5 HTLs (two substrates per HTL comprising 12 pixels). During lifetime testing, a JV sweep (-1.0 V to 1.0 V) was recorded on each pixel every 10 minutes, with the devices held at open circuit between measurements. The devices were tested for a total of 620 hours under constant illumination, during which time they were removed every ~ 3 days to measure EQE and record JV scans under the Newport solar simulator.

In **Figure 2**, we plot the average values PCE, FF, V_{oc} and J_{sc}, determined from the different devices as a function of irradiation time. Here, data recorded using the ATLAS xenon lamp is plotted using blue, red and green lines for MoO_x, PEDOT:PSS and V_2O_5 HTL-based devices respectively. In each figure, we also plot data recorded using the Newport solar simulator with solid symbols using the same colour scheme. In all cases, PCE is normalised to its initial value. Notably, there is a discrepancy between data recorded between ATLAS and Newport systems that derives both from the spectral mismatch between the systems and the fact that an aperture mask was not used to define that active area during measurements in the ATLAS system. For this reason, data recorded using the ATLAS system is only included to highlight general trends in device metrics as they undergo aging.

It can be seen that all devices undergo a burn in phase that lasts for ~ 250 hours in which the FF and J_{sc} decrease at an exponential rate, after which the decay follows a linear trend. We make a

linear-fit to the PCE data post burn-in plotted using a dashed line that allows us to determine the T_{80} lifetime (defined as the point at which the efficiency of the device falls below 80% of its efficiency at the end of the burn-in period).

In **Table 1** we display the average values of PCE, peak EQE, FF, V_{oc} and J_{sc} (and their uncertainties) for all devices before and after lifetime testing (determined using the Newport solar simulator), with corresponding JV and EQE curves shown in **Figure 3**. We also report device PCE after the burn-in period and the relative loss in the PCE after 250 and 620 hours and T_{80} in **Table 2**. The initial burn-in (see **Figure 2**) is believed to originate from photochemical reactions in the PCDTBT:$PC_{70}BM$ blend that adversely affect its charge transport properties [6,11,18,33]. The EQE spectra recorded before and after irradiation (see **Figure 3 (b)** and **(d)** respectively), indicate a general reduction in quantum efficiency commensurate with the observed reduction in J_{sc} without any change in spectral shape; a result consistent with some photooxidation. Here, photochemical reactions in PCDTBT result in an increase in the density of sub-bandgap states that lead to a reduction in hole mobility [11]. The formation of trap states saturates over time, which results in an end to the burn-in phase and subsequent linear decay [11].

It can be seen in **Figure 2** that that devices utilising a PEDOT:PSS HTL underwent a rapid, initial burn in phase that was dominated by a reduction in FF and J_{sc} which then stabilised after 60 hours. Significantly, the V_{oc} of such devices also underwent an initial and rapid reduction (over a period 5 hours) but then recovered and stabilised over a period of 200 hours to a value that was some 15 mV higher than the initial V_{oc}. This, we speculate, results from charge transfer from the PEDOT:PSS to the active layer [34,35]; a process that alters the work function of the PEDOT:PSS surface and thus facilitates charge transfer. Note that the PEDOT:PSS used here is known to be acidic (pH ~ 2 [36,37]), and has been shown to react with the ITO anode [38–40], resulting in degradation of device efficiency. It is possible that the use of different grades of PEDOT:PSS having a more neutral pH may well reduce the drop in efficiency during the initial burn-in period.

We find that the PCE, FF, J_{sc}, and V_{oc} of devices based on MoO_x or V_2O_5 HTLs degraded at a significantly faster rate than that of the PEDEOT:PSS based devices, both during the burn-in period and in the subsequent linear decay. In MoO_x HTL devices, the overall reduction in PCE is dominated by a reduction in FF and J_{sc}, with the V_{oc} only undergoing a relatively small reduction (by 4%) over 620 hours. At present, the precise mechanisms by which the MoO_x HTLs undergo degradation is unclear, however we speculate that such nanocrystalline metal-oxide films undergo thermally-assisted break-down followed by diffusion into the active semiconductor layer; a process that could result in both charge trapping and reduced hole-extraction efficiency.

In V_2O_5 HTL devices, the V_{oc} reduced by 40% over the 620 hours of testing. This reduction was also accompanied by significant reductions in PCE, FF and J_{sc}, as can be seen in **Table 1**, resulting in the largest loss in device PCE. We note that the vanadium oxytriisopropoxide precursor is a Lewis acid, and has been shown to damage conjugated polymers, resulting in the formation of main-chain defects and trap states and a reduction in device PCE [41]. We speculate that residues of the precursor material in the HTL film, along with other organic by-products of the hydrolysis process, may be the cause of such device degradation. This suggests that the use of V_2O_5 HTLs prepared by this synthetic process would be problematic for practical applications. The use of other techniques to deposit V_2O_5 layers [41–44] may address this issue.

In **Table 2**, we display the values for T_{80} that we have extracted from our measurements from the Suntest and Newport solar simulators. The discrepancy between the extrapolated lifetimes results from differences in the PCE as a result of the spectral mismatch and the use of an aperture mask. Using the Newport solar simulator we determine an average lifetime for devices using a PEDOT:PSS HTL of 14,500 hours. If we neglect other possible catastrophic device degradation processes (e.g. failure of the device encapsulation), our extrapolated lifetime is equivalent to 7.2 years of practical operation, assuming an operational device would receive 5.5 hours of sun per day at one sun intensity [6]. For MoO_x, however, the device T_{80} lifetime was found to be 1000 hours (equivalent to 6 months operation); a value reduced to 350 hours (63 days) for the V_2O_5 HTL devices. We emphasise that lifetime figures we determine here are for devices aged indoors under the ISOS-L-1 specification [45], as outdoor testing results in thermal cycling and light intensity variations.

Our experiments demonstrate therefore that the rate of degradation of the device metrics is a significant function of the nature of the HTL material; a result that confirms that degradation in the active layer does not completely account for the observed reduction in device performance. Rather, the changes in FF, J_{sc}, and V_{oc} that we observe also result from the formation of additional trap states at the interface between the active layer and the hole transport layers, due to generation of structural and electronic defects [18].

We have shown therefore that OPV devices utilising a PEDOT:PSS HTL have a higher stability than comparable devices using a MoO_x or V_2O_5 HTLs, with extrapolated T_{80} lifetimes for devices utilising a PEDOT:PSS HTL being 14,500 hours. Such lifetimes are in good accord with the results of previous studies [6]. Other work [9,10,12] however has suggested that OPVs having a PEDOT:PSS HTLs have relatively poor operational stability. We believe this apparent contradiction results from the differing sensitivity of the donor-polymer to trapped moisture. We note that previous studies explored OPVs based on the polymer P3HT; a material known to be sensitive to

the presence of moisture that is likely introduced into the device by the highly hygroscopic PEDOT:PSS [46]. In contrast, however, PCDTBT is more stable to the presence of water and oxygen even under elevated temperatures [11], and thus the effect of trapped moisture within the PEDOT:PSS appears less problematic.

We thank the UK EPSRC for supporting this research through grants EP/I028641/1, EP/J017361/1, EP/I032541/1 and the E-Futures Doctoral Training Centre in Interdisciplinary Energy Research EP/G037477/1.

References

[1] C.J. Brabec, S. Gowrisanker, J.J.M. Halls, D. Laird, S. Jia, and S.P. Williams, Adv. Mater. **22**, 3839 (2010).

[2] M. Jørgensen, K. Norrman, S.A. Gevorgyan, T. Tromholt, B. Andreasen, and F.C. Krebs, Adv. Mater. **24**, 580 (2012).

[3] R. De Bettignies, J. Leroy, M. Firon, and C. Sentein, Synth. Met. **156**, 510 (2006).

[4] J.A. Hauch, P. Schilinsky, S.A. Choulis, R. Childers, M. Biele, and C.J. Brabec, Sol. Energy Mater. Sol. Cells **92**, 727 (2008).

[5] M.O. Reese, A.J. Morfa, M.S. White, N. Kopidakis, S.E. Shaheen, G. Rumbles, and D.S. Ginley, Sol. Energy Mater. Sol. Cells **92**, 746 (2008).

[6] C.H. Peters, I.T. Sachs-Quintana, J.P. Kastrop, S. Beaupré, M. Leclerc, and M.D. McGehee, Adv. Energy Mater. **1**, 491 (2011).

[7] S.A. Gevorgyan, M. V. Madsen, H.F. Dam, M. Jørgensen, C.J. Fell, K.F. Anderson, B.C. Duck, A. Mescheloff, E.A. Katz, A. Elschner, R. Roesch, H. Hoppe, M. Hermenau, M. Riede, and F.C. Krebs, Sol. Energy Mater. Sol. Cells **116**, 187 (2013).

[8] H. Cao, W. He, Y. Mao, X. Lin, K. Ishikawa, J.H. Dickerson, and W.P. Hess, J. Power Sources **264**, 168 (2014).

[9] E. Voroshazi, B. Verreet, A. Buri, R. Müller, D. Di Nuzzo, and P. Heremans, Org. Electron. **12**, 736 (2011).

[10] C. Girotto, E. Voroshazi, D. Cheyns, P. Heremans, and B.P. Rand, ACS Appl. Mater. Interfaces **3**, 3244 (2011).

[11] C.H. Peters, I.T. Sachs-Quintana, W.R. Mateker, T. Heumueller, J. Rivnay, R. Noriega, Z.M. Beiley, E.T. Hoke, A. Salleo, and M.D. McGehee, Adv. Mater. **24**, 663 (2012).

[12] Y. Sun, C.J. Takacs, S.R. Cowan, J.H. Seo, X. Gong, A. Roy, and A.J. Heeger, Adv. Mater. **23**, 2226 (2011).

[13] D.C. Watters, J. Kingsley, H. Yi, T. Wang, A. Iraqi, and D. Lidzey, Org. Electron. **13**, 1401 (2012).

[14] T. Wang, A.J. Pearson, A.D.F. Dunbar, P.A. Staniec, D.C. Watters, H. Yi, A.J. Ryan, R.A.L. Jones, A. Iraqi, and D.G. Lidzey, Adv. Funct. Mater. **22**, 1399 (2012).

[15] S.H. Park, A. Roy, S. Beaupré, S. Cho, N. Coates, J.S. Moon, D. Moses, M. Leclerc, K. Lee, and A.J. Heeger, Nat. Photonics **3**, 297 (2009).

[16] J. Liu, S. Shao, G. Fang, B. Meng, Z. Xie, and L. Wang, Adv. Mater. **24**, 2774 (2012).

[17] Y. Sun, J.H. Seo, C.J. Takacs, J. Seifter, and A.J. Heeger, Adv. Mater. **23**, 1679 (2011).

[18] E. Voroshazi, I. Cardinaletti, T. Conard, and B.P. Rand, Adv. Energy Mater. (2014).

[19] Q. Wei, M. Mukaida, Y. Naitoh, and T. Ishida, Adv. Mater. **25**, 2831 (2013).

[20] J. Huang, P.F. Miller, J.S. Wilson, A.J. de Mello, J.C. de Mello, and D.D.C. Bradley, Adv. Funct. Mater. **15**, 290 (2005).

[21] H. Ding, Y. Gao, C. Small, D.Y. Kim, J. Subbiah, and F. So, Appl. Phys. Lett. **96**, 243307 (2010).

[22] N. Miyata, T. Suzuki, and R. Ohyama, Thin Solid Films **281-282**, 218 (1996).

[23] C.V. Ramana, V.V. Atuchin, V.G. Kesler, V.A. Kochubey, L.D. Pokrovsky, V. Shutthanandan, U. Becker, and R.C. Ewing, Appl. Surf. Sci. **253**, 5368 (2007).

[24] L. Chen, P. Wang, F. Li, S. Yu, and Y. Chen, Sol. Energy Mater. Sol. Cells **102**, 66 (2012).

[25] F. Liu, S. Shao, X. Guo, Y. Zhao, and Z. Xie, Sol. Energy Mater. Sol. Cells **94**, 842 (2010).

[26] S. Murase and Y. Yang, Adv. Mater. **24**, 2459 (2012).

[27] S. Cho, J.H. Seo, S.H. Park, S. Beaupré, M. Leclerc, and A.J. Heeger, Adv. Mater. **22**, 1253 (2010).

[28] K. Zilberberg, S. Trost, H. Schmidt, and T. Riedl, Adv. Energy Mater. **1**, 377 (2011).

[29] I. Hancox, L.A. Rochford, D. Clare, M. Walker, J.J. Mudd, P. Sullivan, S. Schumann, C.F. Mcconville, and T.S. Jones, J. Phys. Chem. C **117**, 49 (2013).

[30] G. Terán-Escobar, J. Pampel, J.M. Caicedo, and M. Lira-Cantú, Energy Environ. Sci. **6**, 3088 (2013).

[31] Y.-M. Chang and J.-M. Ding, Thin Solid Films **520**, 5400 (2012).

[32] N. Blouin, A. Michaud, and M. Leclerc, Adv. Mater. **19**, 2295 (2007).

[33] M.O. Reese, A.M. Nardes, B.L. Rupert, R.E. Larsen, D.C. Olson, M.T. Lloyd, S.E. Shaheen, D.S. Ginley, G. Rumbles, and N. Kopidakis, Adv. Funct. Mater. **20**, 3476 (2010).

[34] C. Perlov, W. Jackson, C. Taussig, S. Mo, and S.R. Forrest, **426**, 2 (2003).

[35] R.A. Nawrocki, E.M. Galiger, D.P. Ostrowski, B.A. Bailey, X. Jiang, R.M. Voyles, N. Kopidakis, D.C. Olson, and S.E. Shaheen, Org. Electron. **15**, 1791 (2014).

[36] M. Kuş and S. Okur, Sensors Actuators B Chem. **143**, 177 (2009).

[37] J. Ouyang, C. Chu, F. Chen, Q. Xu, and Y. Yang, J. Macromol. Sci. Part A **41**, 1497 (2004).

[38] T.P. Nguyen and S.A. de Vos, Appl. Surf. Sci. **221**, 330 (2004).

[39] K.W. Wong, H.L. Yip, Y. Luo, K.Y. Wong, W.M. Lau, K.H. Low, H.F. Chow, Z.Q. Gao, W.L. Yeung, and C.C. Chang, Appl. Phys. Lett. **80**, (2002).

[40] M.P. de Jong, L.J. van IJzendoorn, and M.J.A. de Voigt, Appl. Phys. Lett. **77**, 2255 (2000).

[41] K. Zilberberg, S. Trost, J. Meyer, A. Kahn, A. Behrendt, D. Lützenkirchen-Hecht, R. Frahm, and T. Riedl, Adv. Funct. Mater. **21**, 4776 (2011).

[42] Z. Tan, W. Zhang, C. Cui, Y. Ding, D. Qian, Q. Xu, L. Li, S. Li, and Y. Li, Phys. Chem. Chem. Phys. **14**, 14589 (2012).

[43] J.-S. Huang, C.-Y. Chou, M.-Y. Liu, K.-H. Tsai, W.-H. Lin, and C.-F. Lin, Org. Electron. **10**, 1060 (2009).

[44] F. Xie, W.C.H. Choy, C. Wang, X. Li, S. Zhang, and J. Hou, Adv. Mater. **25**, 2051 (2013).

[45] M.O. Reese, S.A. Gevorgyan, M. Jørgensen, E. Bundgaard, S.R. Kurtz, D.S. Ginley, D.C. Olson, M.T. Lloyd, P. Morvillo, E.A. Katz, A. Elschner, O. Haillant, T.R. Currier, V. Shrotriya, M. Hermenau, M. Riede, K. R. Kirov, G. Trimmel, T. Rath, O. Inganäs, F. Zhang, M. Andersson, K. Tvingstedt, M. Lira-Cantu, D. Laird, C. McGuiness, S. (Jimmy) Gowrisanker, M. Pannone, M. Xiao, J. Hauch, R. Steim, D.M. DeLongchamp, R. Rösch, H. Hoppe, N. Espinosa, A. Urbina, G. Yaman-Uzunoglu, J.-B. Bonekamp, A.J.J.M. van Breemen, C. Girotto, E. Voroshazi, and F.C. Krebs, Sol. Energy Mater. Sol. Cells **95**, 1253 (2011).

[46] A.M. Nardes, M. Kemerink, M.M. de Kok, E. Vinken, K. Maturova, and R.A.J. Janssen, Org. Electron. **9**, 727 (2008).

		PCE (%)	**Peak EQE (%)**	**FF**	**V_{oc} (V)**	**J_{sc} ($mAcm^{-2}$)**
Molybdenum Oxide (MoO_x)	Initial	5.19±0.07	54.7±0.1	64.6±0.7	0.91±0.01	-8.9±0.1
	Final	2.7±0.1	47.4±0.2	43.9±0.9	0.87±0.01	-7.0±0.2
PEDOT:PSS	Initial	5.6±0.2	63.7±0.2	65.9±0.9	0.85±0.01	-9.9±0.2
	Final	3.4±0.2	56.6±0.3	46±1	0.89±0.001	-8.3±0.4
Vanadium	Initial	5.2±0.2	58.4±0.1	65±1	0.85±0.01	-9.4±0.1

Oxide (V_2O_5)	Final	1.18±0.04	43.7±0.1	36.8±0.8	0.51±0.2	-6.3±0.1

Table 1. Average values for PCE, FF, V_{oc} and J_{sc} were calculated from 12 pixels across two substrates, as measured using the Newport solar simulator, where the worst 25% of pixels were discarded due to film defects. The error quoted on all measurements is based on the standard deviation around the mean.

	PCE after burn-in (250hrs)	**PCE Loss over burn-in (250hrs)**	**PCE Loss over 620 hours**	**T_{80} (hours) Newport**	**T_{80} (hours) Suntest**
Molybdenum Oxide (MoO_x)	2.9±0.1%	44±3%	48±3%	1000	650
PEDOT:PSS Annealed	3.4±0.4%	39±6%	39±5%	14500	20000
Vanadium Oxide (V_2O_5)	1.5±0.1%	72±4%	77±4%	350	236

Table 2. PCE loss on burn in and over the full 620 hrs of testing with calculated T_{80} lifetimes determined using the Newport solar simulator data and the ATLAS Suntest CPS+ data. All PCE values and losses were calculated using data from the Newport solar simulator.

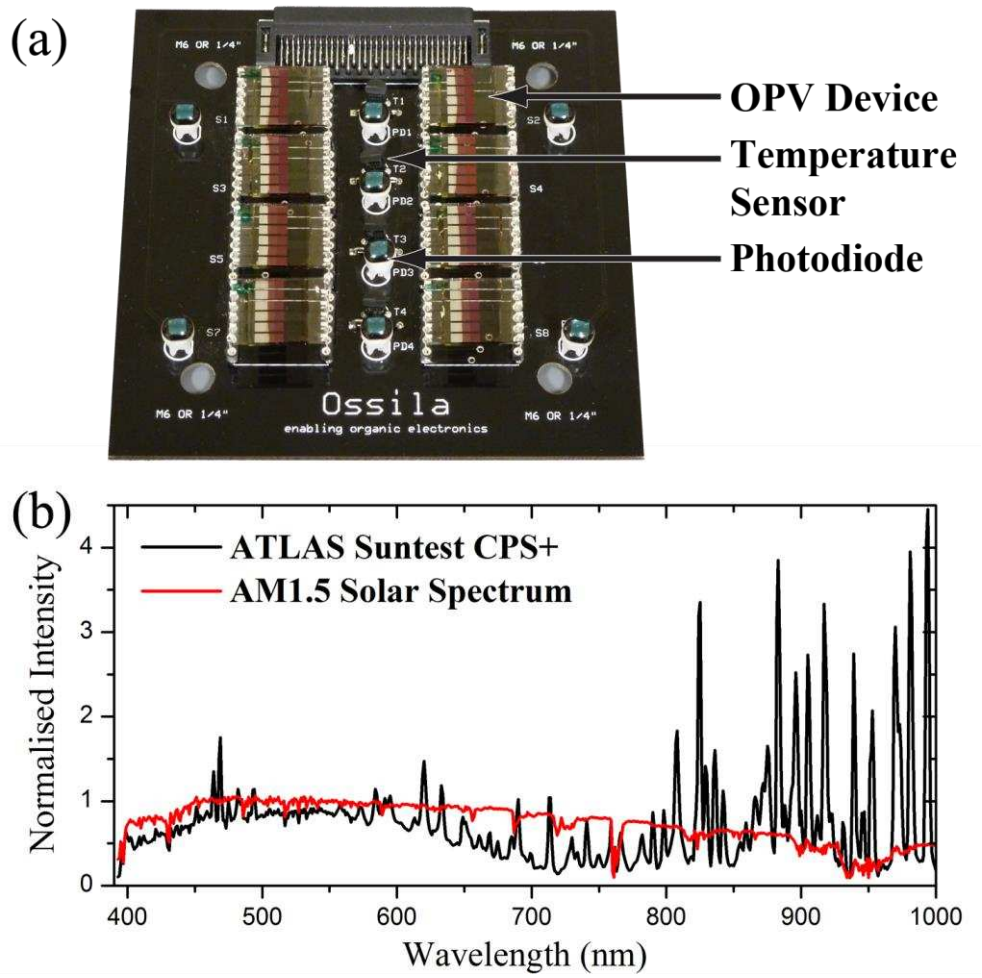

Figure 1. (a) Lifetime test board. (b) Spectrum of the ATLAS Suntest CPS+ and AM1.5 solar spectrum.

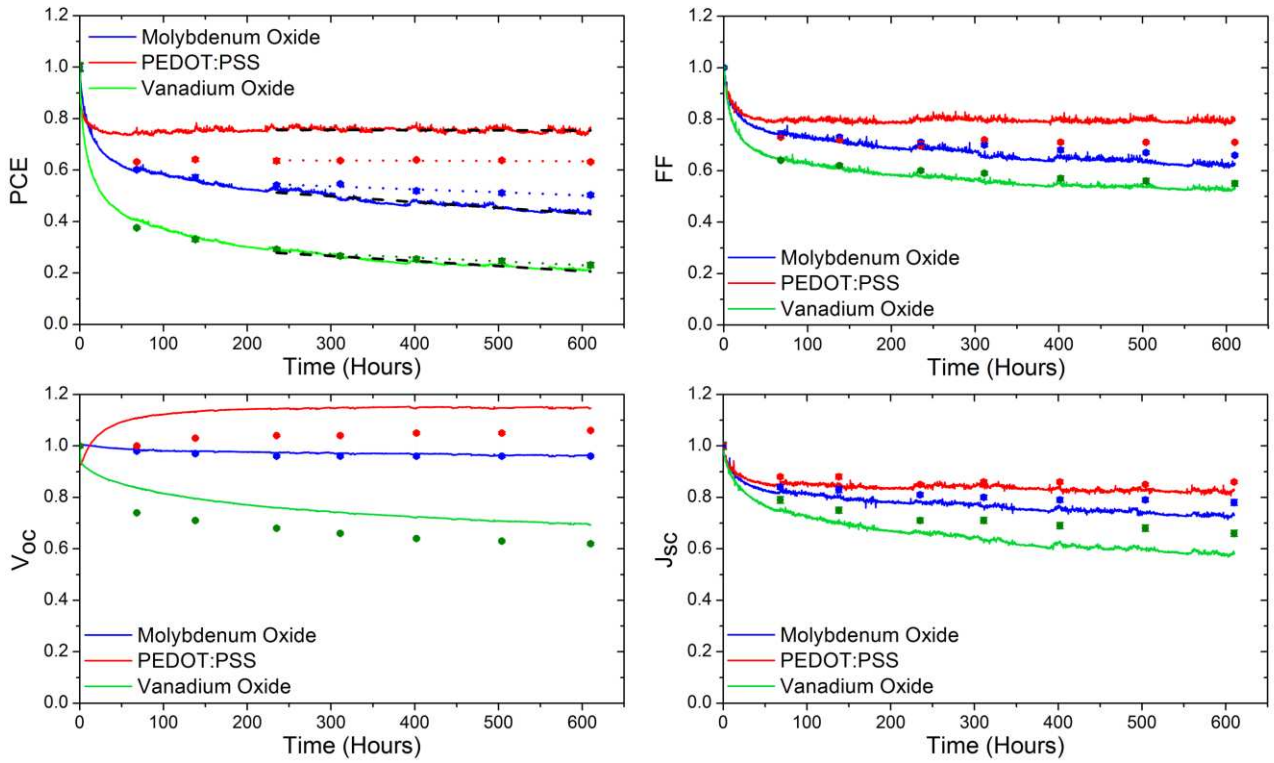

Figure 2 shows PCE, V_{oc}, J_{sc} and FF for devices utilising the different HTL materials as a function of irradiation time under the ATLAS solar simulator. All data is normalised to its initial value determined at t = 0. In each part, we plot data measured every 10 minutes using the ATLAS solar simulator (solid lines) and every 3 days using the calibrated Newport solar simulator (circular data points). The decay in PCE (determined using both types of solar simulator) is fitted to a straight line (dashed line or dotted line) for times beyond the burn-in period (t > 250 hours). This linear fit to the PCE is used to determine the T_{80} decay lifetime.

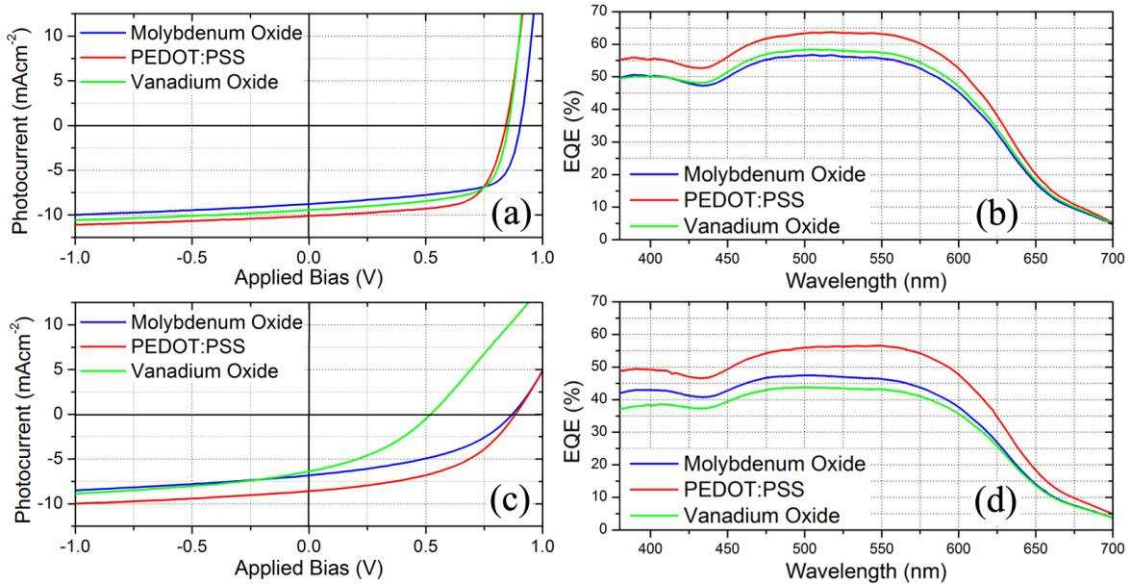

Figure 3. Parts (a) and (b) show initial JV and EQE characteristics for devices respectively, with parts (c) and (d) showing device JV and EQE characteristics after 620 hours of irradiation under the ATLAS solar simulator.